Statistical Analysis of Radio Interference of 1000 kV UHV AC Double-circuit Transmission Lines in Foul Weather

Huichun Xie, *Member*, *CSEE*, Xiang Cui, *Senior Member*, *IEEE*, Baoquan Wan, *Member*, *CSEE*, and Jiangong Zhang, *Member*, *CSEE*

***Abstract*—Analyzing the impact of radio interference (RI) variation during foul weather conditions is an area that has received limited study. This paper provides a statistical analysis of RI measurements obtained from a long-term observation station close to the world's first commercially operating 1000 kV UHV AC double-circuit transmission line in China. During six months of observations, the impact of RI was studied on the line during fog, drizzle, and light snow and rain. It was found that RI increases linearly with the natural logarithm of the precipitation intensity. The Levenberg-Marquardt algorithm (LMA) is employed to fit the RI value with the precipitation intensity. The reasonable distribution of RI in different foul weather is verified by one-sample K-S test. This test is seen as beneficial for further RI prediction based on statistical weather mode.**

***Index Terms*—1000 kV UHV AC double-circuit transmission line, foul weather, precipitation intensity, radio interference, statistical analysis.**

I. Introduction

RADIO interference (RI) is an important issue to be considered in the design of UHV transmission lines. Research has shown that the RI of an overhead electric line in operation depends on many factors, some constant and others variable in time. The constant factors are related to the geometric and physical characteristics of the line (conductor diameter, number of sub-conductors per phase, etc.). The variable factors concern the working conditions of the line (operating voltage), prevailing atmospheric conditions (fair weather, rain, fog, etc.), and surface conditions of conductors, e.g., presence of insects or polluting agents, in general, as well as surface roughness [1]–[4].

Manuscript received April 28, 2015; revised August 17, 2015 and October 29, 2015; accepted March 23, 2016. Date of publication June 30, 2016; date of current version May 10, 2016. This work was supported in part by the National Basic Research Program (973 Program) under Grant 2011CB209402-3 and the Science and Technology Project of the State Grid Corporation of China under Grant GY71-15-033.

H. C. Xie (corresponding author, e-mail: xiehuichun@epri.sgcc.com.cn) is with State Key Laboratory of Alternate Electrical Power System with Renewable Source (NCEPU), Beijing 102206, China. He is also with the China Electric Power Research Institute, Wuhan 430074, China.

X. Cui is with State Key Laboratory of Alternate Electrical Power System with Renewable Source (NCEPU), Beijing 102206, China.

B. Q. Wan and J. G. Zhang are with the China Electric Power Research Institute, Wuhan 430074, China.

DOI: 10.17775/CSEEJPES.2016.00021

The variable factors are viewed as the most obvious impacts on RI that can in general lead to extreme variations in RI during operation. As a result, the behavior of an operating line with respect to RI may be defined in a complete manner only when the statistical distribution of RI over a sufficiently long period of time is known. In recent literature, RI prediction methods based on statistical weather modes have received some attention [5].

Huainan–Shanghai UHV Project is the world's first 1000 kV UHV AC demonstration project in China that operates on a double-circuit UHV AC transmission line, starting from the city of Huainan of Anhui Province, continuing through the cities of Hefei, Xuancheng, and Jiaxing, and ending in Shanghai (Fig. 1). The length of this line is 656 km. There are plans to construct several such UHV projects in the future in China, but the statistical characteristics of UHV AC lines RI have not yet been determined. To provide basic data for the design of future UHV projects, a long-term observation station has been established around this line at Lujiang County, Hefei.

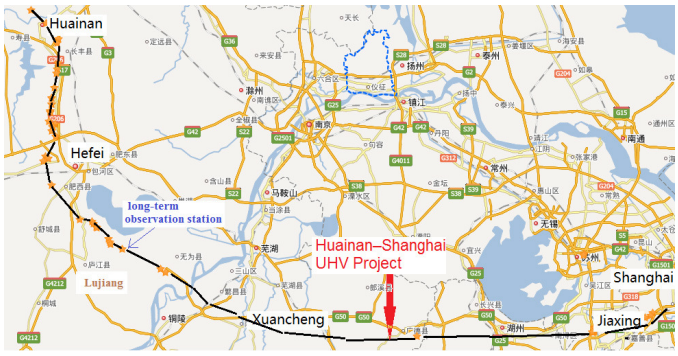

Fig. 1. Chinese Huainan–Shanghai 1000 kV UHV AC double-circuit transmission line.

In earlier works, a common method for RI statistical analysis has been to acquire cumulative frequency distribution diagrams in fair and foul weather derived from long-term measurements [6]–[10]. However, variability in corona excitation sources on conductor surface under different weather conditions leads to corona discharge of varying complexities. Studies thus far have addressed this phenomenon by treating heavy fog, drizzle, rain and snow collectively as "foul weather." While the overall cumulative frequency distribution of RI in foul weather has been examined [11]–[16], there are

no studies related to different foul weather classifications. Most research to date has involved the recording of statistical data from lines, test lines, or corona cage tests of 2.4–765 kV [17]–[20], but there exists no RI data for operating 1000 kV UHVAC double-circuit transmission lines.

This paper reports for the first time the RI of operating a 1000 kV UHVAC double-circuit transmission line in different types of foul weather, and describes the RI variation process based on weather changes. The aim of this paper is to discuss the results of continuous recording obtained in different foul weather between the months of February and July 2015.

II. Description of Research

A. Measuring Device and Layout

The tower parameters for the 1000 kV UHV AC double-circuit transmission line are as shown in Fig. 2. The tower's sub-conductor is LGJ-630/45 with a diameter of 33.6 mm. There are eight sub-conductors in a single bundle, and the spacing between sub-conductors is 400 mm having an operating voltage of 1050 kV. The average maximum potential gradient of the conductor surface of Phase A is 14.44 kV/cm (RMS value). The average maximum gradient of Phase B is 14.82 kV/cm (RMS value), and the average maximum gradient of Phase C is 14.73 kV/cm (RMS value). Based on the excitation function approach in [21], the calculated RI during heavy rain is 71.22 dB at lateral 20 m.

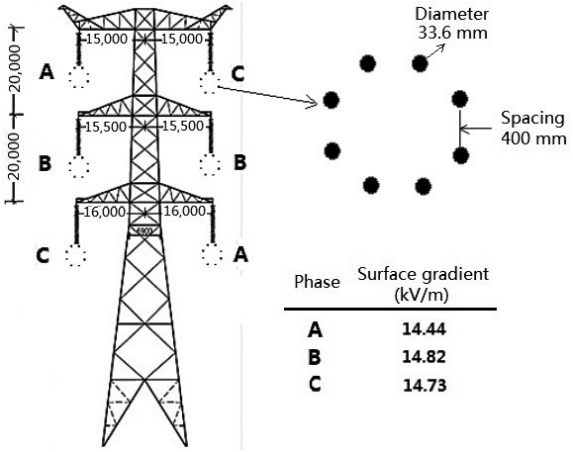

Fig. 2. Tower size of Chinese Huainan–Shanghai 1000 kV UHV AC double-circuit transmission line (dimensions in mm).

The RI measurement instrument used is a FCKL1528 EMI receiver manufactured by SCHWARZBECK Mess-Elektronik, which meets CISPR 16-1-1. Automatic calibration is executed through a built-in pulse generator. The frequency range is 9 kHz–30 MHz. An active receiving loop antenna, ETS 6502, produced by ETS-LINDGREN has been used in the past to receive the magnetic RI field whose frequency range is 10 kHz–30 MHz. A radio frequency preamplifier is built into the base of the antenna and provides 50 Ω output, which is used by a receiver. The preamplifier helps produce good sensitivity and almost constant antenna factors. A loop antenna is individually calibrated in accordance with the IEEE-291 Section 2.3.1 methods, using NIST traceable equipment.

For measuring weather phenomena and atmospheric parameters, SWS200 produced by Bristol Industrial & Research Associates Ltd. (Biral) is employed. The SWS200 measures meteorological optical range (MOR) as well as reports the presence of liquid and frozen precipitation. Precipitation is reported using WMO 4680 present weather codes with which SWS200 can identify and provide outputs for 14 types of weather phenomena.

An ETS6502 is placed below midspan at a position of 20 m lateral and 2 m above the ground (Fig. 3). Brail SWS200 is placed 3 m above the ground (Fig. 4). An ultraviolet instrument is used to detect the spark discharge on the adjacent tower and insulators. To date, no visible spark phenomenon has been found; this excludes the additional effect on RI caused by corona discharge of transmission line.

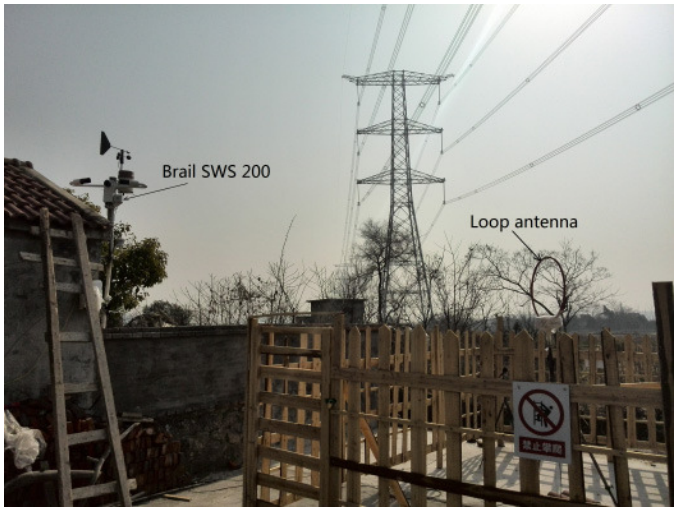

Fig. 3. Loop antenna placed below midspan, 20 m lateral.

Fig. 4. Brai SWS200 placed 3 m above ground.

RI data from FCKL1528 are then sent to a data collecting system on a PC using a USB/GPIB interface on FCKL 1528. Time of storage and clock synchronization is executed through a desktop computer using the FCKL1528 and Brail SWS200 data software. One set of atmospheric parameters is recorded every 5 minutes including the weather code and the accumulated precipitation amounts in a 5-minute period. One

CISPR quasi-peak value of RI at 0.5 MHz is recorded per 20 seconds.

Measured background noise was seen to be approximately 42 dB when the line was out of operation between 30/01/2015 to 02/02/2015. Average RI level in fair weather was about 51 dB, which is 9 dB greater than the background noise, and the spectrum measurement was also executed by which extra interference could be detected from the spectrum characteristics. This suggests that the measurement data are accurate.

B. Weather Classifications

Corona phenomena are drastically affected by the weather. Foul weather conditions have the greatest effect on corona generation, and it is important to have a common understanding of the weather terms that are used. IEEE Standard 539-2205 [22] points out the classification of several weather phenomena:

1) Fair weather: the weather condition when the precipitation intensity is zero and the transmission line is dry.
2) Foul weather: the weather condition when there is precipitation that can cause the transmission line conductors to be wet. Fog is not a form of precipitation, but it causes conductors to be wet.
3) Rain: precipitation in the form of liquid water drops with diameters greater than 0.5 mm or, if widely scattered, smaller diameters. For observation purposes, the intensity of precipitation at any given time and place may be classified as follows:
   a) very light—scattered drops that do not completely wet an exposed surface regardless of duration;
   b) light—the rate of fall being no more than 2.5 mm/h;
   c) moderate—from 2.6 mm/h to 7.6 mm/h;
   d) heavy—over 7.6 mm/h.
4) Fog: visible aggregate of minute water droplets suspended in the atmosphere near the earth's surface. According to the international definition, fog reduces visibility below 1 km.

By observing the ratio of forward to backscatter for each precipitation particle, the SWS-200 provides an accurate assessment of present weather. Obstructed vision and precipitation intensity definitions for Biral SWS200 are as follows:

1) Fog: Meteorological optical range (MOR) is less than 1 km.
2) Haze: MOR is more than 1 km and less than 10 km.
3) Light drizzle: Precipitation amount is less than 0.26 mm/h.
4) Moderate drizzle: Precipitation amount is more than 0.26 mm/h and less than 1.01 mm/h.
5) Heavy drizzle: Precipitation amount is more than 1.01.mm/h.
6) Light snow: MOR is more than 0.8 km.

In this paper, since no accurate definition and threshold about drizzle \snow\haze\fog has been given in the IEEE standard, definitions of these weather phenomena have been adopted according to Biral SWS200. The definition of rain, however, is based on IEEE standard.

Weather phenomenon code outputs using SWS-200 are available in Table I.

TABLE I
WEATHER CODE BY SWS-200

Weather Phenomenon Code	Weather Classification
0	No significant weather observed
4	Haze or smoke
30	Fog
40	Indeterminate precipitation type
51	Light drizzle
52	Moderate drizzle
53	Heavy drizzle
61	Light rain
62	Moderate rain
63	Heavy rain
71	Light snow
72	Moderate snow
73	Heavy snow
89	Hail

The weather code in Table I will be used in the following figures to show the relationship between RI and weather phenomena.

According to the IEEE standard, on a rainy day, the weather phenomenon in which 5 m accumulated precipitation amount is less than $2.5/60 \times 5 = 0.208$ mm will be treated as light rain; the weather phenomenon in which 5 m accumulated precipitation amount is between $7.6/60 \times 5 = 0.633$ mm and 0.208 mm will be treated as moderate rain, while 5 m of accumulated precipitation amount is more than 0.633 mm will be treated as heavy rain.

III. RI VARIATION PROCESS WITH THE WEATHER PROCESS

From February to July 2015, RI data during the following foul weather was recorded: 74 rainy days, 6 rainy days mixed with fog, 10 fog days, and 1 light snow day. Here, a rainy day means in that day it might drizzle, rain, or both.

First, an analysis was conducted on the RI variation process based on weather and time. The output provided further understanding of RI behavior in foul weather.

A. Fog

Fog occurred on the following dates: 16/02/2015, 08/04/2015, 17/04/2015, 21/04/2015, 24/04/2015, 07/05/2015, 18/05/2015, 19/05/2015, 09/06/2015, 24/06/2015. No liquid precipitation was detected. The main weather phenomena during those days were fog, haze, and no significant other weather event. Fig. 5 shows that the typical RI value changed from haze to fog, and then to haze again during different months.

Different from RI during fair weather, RI in foggy weather appears unstable with many pulses occurring above basic values, with maximum variations reaching over 10 dB. It seems that before the beginning of fog, RI value fluctuated sharply and then rose. The oscillation amplitude and frequency of RI then tended to be less than that in the beginning and RI gradually reduced with the fog process. In other words, the RI value keeps relatively stable until the fog disappears. The line curves in Fig. 5 also show probable positive correlations between the RI value and the meteorological optical range with fog process.

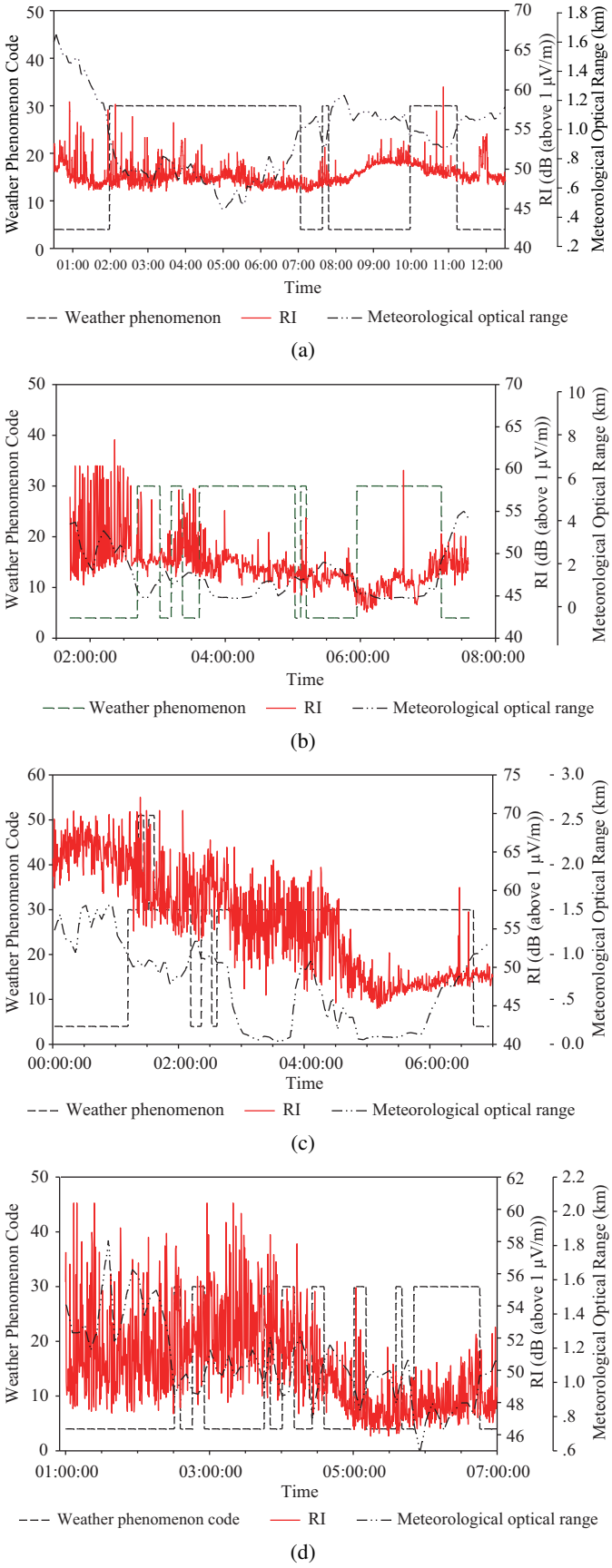

Fig. 5. RI value changes with fog process. (a) Fog day, 16/ 02/2015. (b) Fog day, 08/04/2015. (c) Fog day, 07/05/2015. (d) Fog day, 09/06/2015.

B. Light Snow

Light snow occurred on February 19, 2015. On that day, the weather phenomena changed from "no significant weather observed" to "light snow," and then the light snow disappeared. Light snow lasted for about 25 minutes. Fig. 6 shows the RI variation before, after, and during the light snow process. Also the accumulated precipitation amounts of 5 m, which is minimal, have been given in this figure. From Fig. 6, it is easy to see that the changes in RI tend to be minimal with light snow, and RI almost does not change with the precipitation under 0.03 mm/5 m.

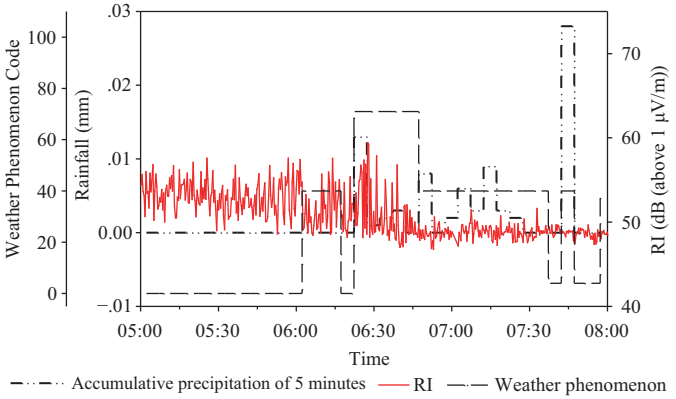

Fig. 6. RI value changed with light snow process and precipitation, light snow day, 19/02/2015.

C. Rain

1) RI vs. Rain Process

Seventy-four rainy days, including light rain, moderate rain, and heavy rain were recorded. Fig. 7 gives the typical RI change line curve in the natural rain process, which includes light rain, light rain-moderate rain-light rain, and light rain-moderate rain-heavy rain-moderate rain-light rain. RI typically changed with precipitation demonstrating that RI is affected by precipitation.

The rainy day records indicate that RI will gradually increase about one hour before precipitation can be measured. This may be due to the fact that extremely tiny water drops gradually form at the bottom of the conductors, which leads to corona spark even though no precipitation has been measured. RI almost synchronously changes during rainfall because the number of discharge points on conductor surface is closely related to the amount of precipitation. When the precipitation drops to zero, RI drops immediately.

It seems that RI comes to an extremely low value within one hour after no precipitation is measured. However, RI does not remain unchanged after dropping to the extremely low value, experiencing a small increase thereafter. The explanation for this phenomenon may be that the conductor surface was cleaned by the rain's washing effect, and then subsequently it dried up as a result of load current heating, leading to some particles (like dust in air) gradually adhering to the conductor surface to increase the RI. However, this observation requires further microscopic study to arrive at a more accurate explanation.

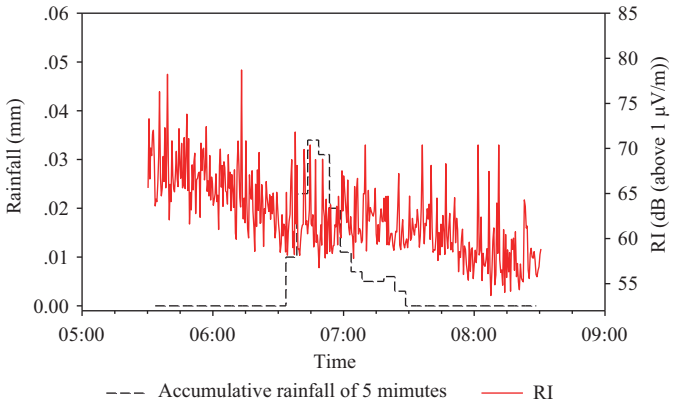

(a)

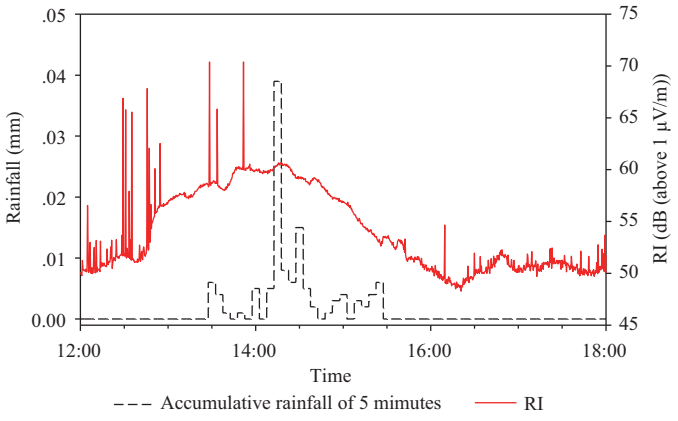

(b)

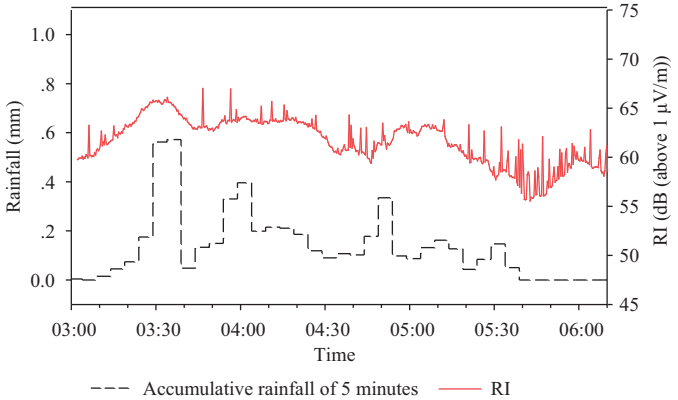

(c)

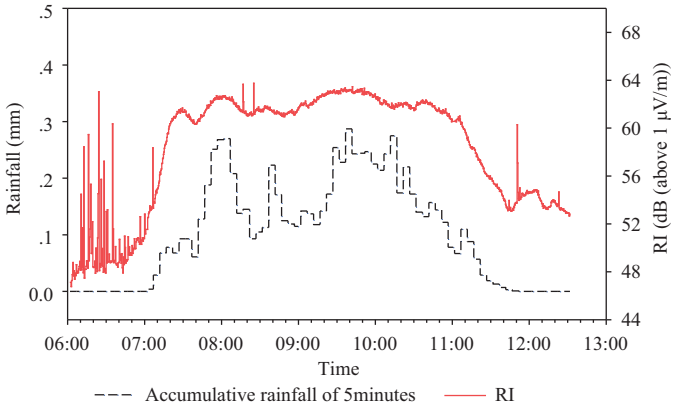

(d)

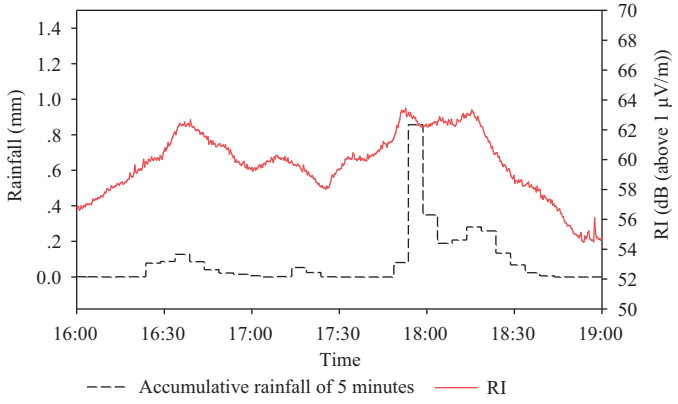

(e)

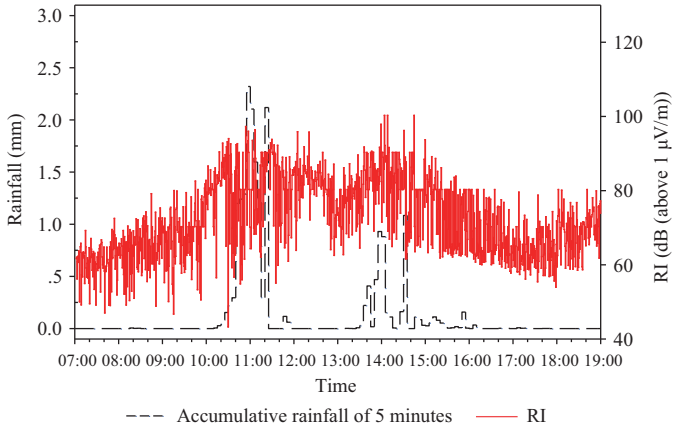

(f)

Fig. 7. RI value changed with rain process and precipitation. (a) Light rain, 04/04/2015. (b) Light rain, 04/05/2015. (c) Light–moderate–light rain, 15/02/2015. (d) Light–moderate–light rain, 20/02/2015. (e) Light–moderate–heavy–moderate–light rain, 27/02/2015. (f) Light–moderate–heavy–moderate–light rain, 17/03/2015.

Curves in Fig. 7(b) show that the RI value may be from 50 dB to 65 dB and can possibly change to about 15 dB even on light rain days. During light rain-moderate to rain-light rain conditions, RI tends to be more stable with less oscillations than in light rain. This indicates that corona discharge in moderate rain is stable.

2) *RI vs. Precipitation Intensity*

Average value of RI for a period of rainy time was calculated. The precipitation intensity is the total average precipitation amount of that period of rainy time. Total data size is 54 including 19 light rain days, 22 moderate rain days and 13 heavy rain days.

Fig. 8 shows a scatter graph of average values of RI vs. precipitation intensity. The Levenberg-Marquardt algorithm (LMA) is employed to fit the RI value with the precipitation intensity [23], [24]. LMA provides a numerical solution to the problem of minimizing a function, generally nonlinear, over the function parameter space. The primary application of the LMA is in the least squares curve fitting problem: given a set of empirical data pairs of independent and dependent variables, (x_i, y_i), optimize the parameters $\boldsymbol{\beta}$ of the model curve $f(x, \beta)$ so that the sum of the squares of the deviations $S(\beta)$ becomes

minimal.

$$S(\beta) = \sum_{i=1}^{m} [y_i - f(x_i, \beta)]^2. \tag{1}$$

In each iteration, the parameter vector $\boldsymbol{\beta}$ is replaced by a new estimate, $\beta + \delta$. To determine δ, the functions are approximated by their linearizations,

$$f(x_i, \beta + \delta) \approx f(x_i, \beta) + J_i \delta \tag{2}$$

$$J_i = \frac{\partial f(x_i, \beta)}{\partial \beta} \tag{3}$$

where J_i is the gradient of f with respect to β,

$$J = \begin{bmatrix} \frac{\partial y_1}{\partial x_1} & \cdots & \frac{\partial y_1}{\partial x_n} \\ \vdots & \ddots & \vdots \\ \frac{\partial y_m}{\partial x_1} & \cdots & \frac{\partial y_m}{\partial x_n} \end{bmatrix} \tag{4}$$

$$(\mathbf{J}^{\mathrm{T}}\mathbf{J} + \lambda \mathbf{I})\delta = \mathbf{J}^{\mathrm{T}}[\mathbf{y} - \mathbf{f}(\beta)] \tag{5}$$

where $\mathbf{J}$ is the Jacobian matrix whose i^{th} row equals J_i, and where $\mathbf{f}$ and $\mathbf{y}$ are vectors with i^{th} component $f(x_i, \beta)$ and y_i, respectively. This is a set of linear equations that can be solved for δ. where $\mathbf{I}$ is the identity matrix, given as the increment, δ, to the estimated parameter vector, $\boldsymbol{\beta}$.

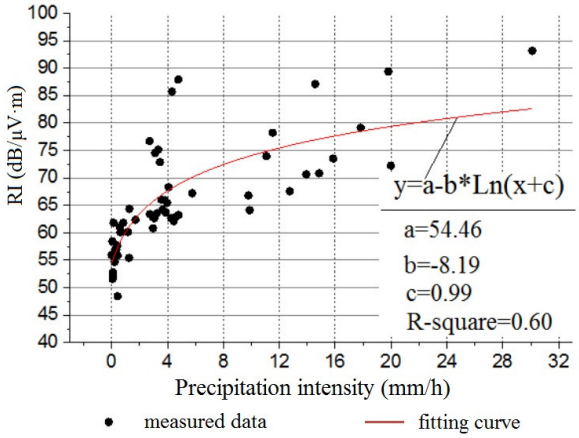

Fig. 8. RI vs. precipitation intensity.

The fitting formula is also illustrated in Fig. 8, showing that RI increases linearly with the natural logarithm of the precipitation intensity. The line in Fig. 8 is the calculated curve according to the fitting formula. The R-square of the fitting is 0.60, so not so close to 1, but for the dispersion of RI from very light rain to extremely heavy rain, it is acceptable for this fitting. Fig. 9 shows the normal probability plot of the residuals in which the scatters are close to the straight line, indicating a good fitting. The derivation of this fitting formula is (6), which denotes that the magnitude of increase of RI increases reciprocally with the precipitation intensity growth.

$$\partial y = \frac{b}{x + c} \partial x \tag{6}$$

Based on the IEEE standard, the fitting formula can be calculated as follows: for light rain, RI is less than 64.70 dB; for moderate rain, RI is between 64.70 dB and 72.06 dB; for heavy rain, RI is more than 72.06 dB, which is larger than the calculated value using the CISPR approach. Even in heavy rain, RI might change from 72 dB to 82 dB, which is not stable, so a statistical analysis is also necessary.

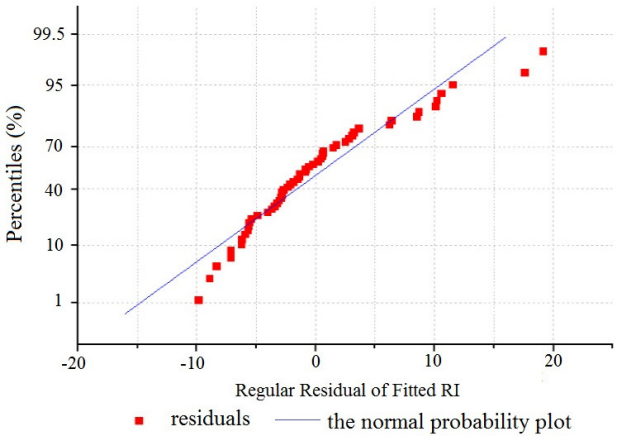

Fig. 9. The normal probability plot of the residuals.

IV. Statistical Analysis of RI in Foul Weather

Total RI records of 14 fog days, 19 light rain days, 22 moderate rain day and 13 heavy rain days were analyzed.

The one-sample Kolmogorov–Smirnov test (K-S test) was employed to conduct the nonparametric testing of the empirical distribution function (EDF) of the sample, and the cumulative distribution function (CDF) of the theoretical distribution, which measures how well the sample data follows a particular distribution [25], [26].

K-S test is a nonparametric test of the null hypothesis in which the EDF of the data is equal to the theoretical CDF. The two-sided test for "unequal" CDF functions tests the null hypothesis against the alternative where the EDF of the data is not equal to the hypothesized theoretical CDF. The test statistic is the maximum absolute difference between the EDF calculated from the samples and the hypothesized CDF:

$$D^* = \max_x(|\hat{F}(x) - G(x)|) \tag{7}$$

where $\hat{F}(x)$ is the EDF and $G(x)$ is the CDF of the hypothesized distribution.

The p-value of the test is returned as a scalar value in the range [0, 1]. p is the probability of observing a test statistic as extreme, or more extreme than the observed value under the null hypothesis. Small values of p cast doubt on the validity of the null hypothesis. The K-S test decides to reject the null hypothesis by comparing the p-value p with the significance level α. In this paper $\alpha = 0.02$. In case of p-value p greater than α, we accept the null hypothesis that the sample data comes from the hypothesized distribution.

For each fog day, K-S test has been utilized to acquire the suitable distribution. Fig. 10 shows the typical histogram of RI value on fog days. In Fig. 10 the curve is the probability density function of 4-parameter Burr distribution whose

expression is as follows:

$$PDF_{\text{4-parameter Burr}}(x) = \frac{\alpha k(\frac{x-\gamma}{\beta})^{\alpha-1}}{\beta(1+(\frac{x-\gamma}{\beta})^{\alpha})^{k+1}}. \quad (8)$$

The p-value $p = 0.33986$ in Fig. 10 is greater than $\alpha = 0.02$. Fig. 11 is the P-P plot of the same RI data which also confirm that RI on 08/04/2015, the fog day, follows 4-parameter Burr distribution. All 14 fog days tested for RI using the K-S test indicate that 4-parameter Burr distribution is suitable.

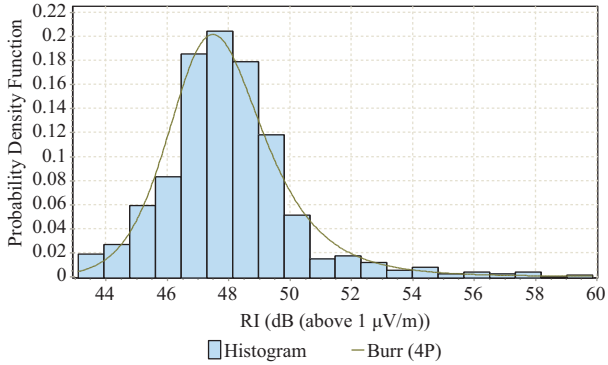

Fig. 10. Histogram of RI value on fog day, 08/04/2015.

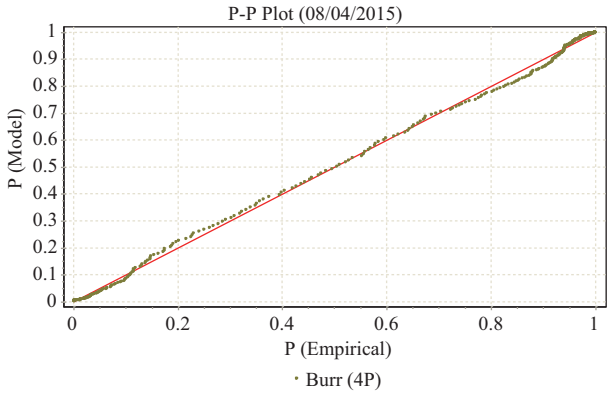

Fig. 11. P-P plot, by EDF values of RI plotted against the theoretical CDF.

As for RI data in light rain, due to great dispersion, no uniform distribution could be found to describe the statistical characteristic. Fig. 12 shows RI histogram values on a light day, 19/04/2015. In Fig. 12 the curve is the probability density function of generalized extreme value distribution.

RI value of each moderate rain day was tested, and for about 82% of moderate rain days, the Johnson SB distribution is seen as reasonable. The distribution formula is as follows:

$$PDF_{\text{Johnson SB}}(x) = \frac{\delta}{\lambda\sqrt{2\pi}z(1-z)} \exp(-\frac{1}{2}(\gamma+\delta\ln(\frac{z}{1-z}))^2). \quad (9)$$

Fig. 13 shows the typical histogram of RI value on a moderate rain day in which the curve is the probability density function of the Johnson SB distribution. The p-value $p = 0.67916$ of Fig. 13 is greater than $\alpha = 0.02$.

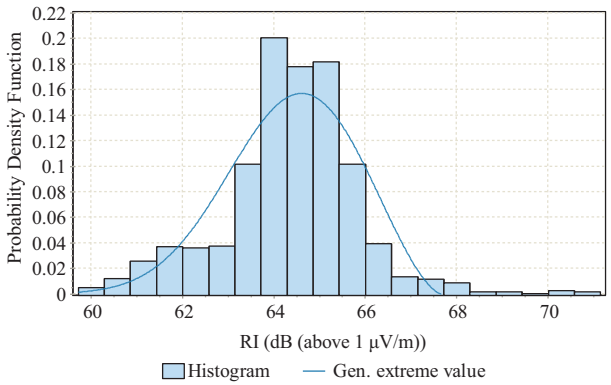

Fig. 12. Histogram of RI value on light rain day, 19/04/2015.

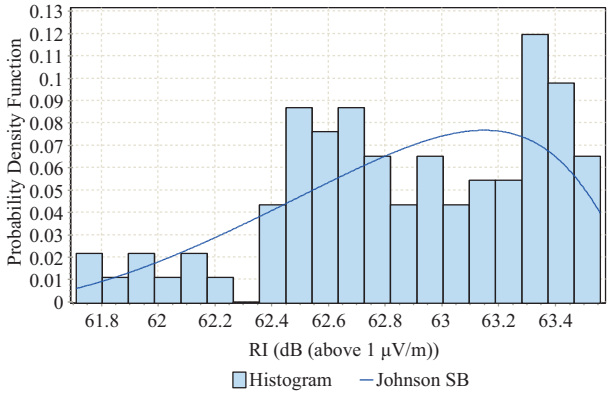

Fig. 13. Histogram of RI value on moderate rain day, 09/07/2015.

RI value on each heavy rain day was tested, and for about 75% of heavy rain days, 3-parameter log-logistic distribution was found to be suitable, whose formula is as follows;

$$PDF_{\substack{\text{3-parameter}\\ \text{log-logistic}}}(x) = \frac{\alpha}{\beta}(\frac{x-\gamma}{\beta})^{\alpha-1}(1+(\frac{x-\gamma}{\beta})^{\alpha})^{-2}. \quad (10)$$

Fig. 14 shows the typical RI histogram value on a heavy rain day in which the curve is the probability density function of 3-parameter log-logistic distribution. The p-value $p = 0.95064$ of Fig. 14 is greater than $\alpha = 0.02$.

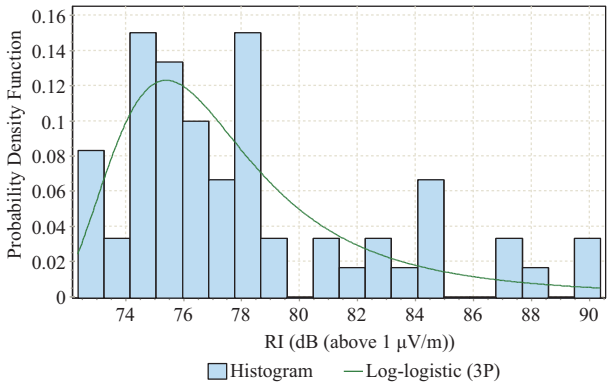

Fig. 14. Histogram of RI value on heavy rain day, 15/05/2015.

It is well known that RI prediction under all-weather conditions is based on weather mode in statistical terms, obtained

from different weather condition. The aforementioned distributions will contribute to further RI prediction of UHV AC transmission lines.

V. Conclusion

The RI of 1000 kV UHV AC double-circuit transmission line during several foul weather days in 6 months, including 74 rainy days, 6 rainy days mixed with fog, 10 fog days, and 1 light snow day, is reported in this paper. The RI variation process with changes in the weather process and the statistical characteristics of RI are also discussed as follows:

1) RI during fog appears is unstable and above the normal pulses range, indicating there may be a positive correlation between RI value and the meteorological optical range of fog processes.
2) RI is definitively affected by precipitation in the form of rain. RI will gradually increase about one hour before precipitation can be measured. When the rainfall drops to zero, RI drops immediately. It seems that RI comes to an extremely low value in one hour after no precipitation is measured and even then there is only a small increase.
3) The Levenberg-Marquardt algorithm (LMA) is employed to fit the RI value with the precipitation intensity. According to this fitting formula, RI increases reciprocally with precipitation intensity growth.
4) Even in heavy rain, RI is not stable and may change from 72 dB to 82 dB, which is a larger range than the calculated value of 71.22 dB in the CISPR approach; therefore further statistical analysis is still necessary.
5) The one-sample K-S test is employed to find the reasonable distribution of RI in different foul weather. 4-parameter Burr distribution, Johnson SB distribution and 3-parameter log-logistic distribution are all suitable measurements for RI during fog, moderate rain, and heavy rain, respectively.

Acknowledgment

The authors are grateful to the Chinese Electric Power Research Institute for the funding support for measurement and acknowledge the contribution Mr. Huagang Liu, Mr. Zhenghuan Liu, Mr. Hao Wan, and Mr. Yulong Chen of Chinese Electric Power Research Institute who set up the measuring instruments and data processing.

References

[1] G. W. Juette, H. Charbonneau, H. I. Dobson, C. Gary, N. Kolcio, M. Moreau, J. Reichman, and E. R. Taylor, "CIGRE/IEEE survey on extra high voltage transmission line radio noise," *IEEE Transactions on Power Apparatus and Systems*, vol. 92, no. 3, pp. 1019–1028, May 1973.

[2] *Radio Interference Characteristics of Overhead Power Lines and High-Voltage Equipment, Part 1: Description of Phenomena*, CISPR 18-1, 1982.

[3] J. R. Leslie, B. M. Bailey, L. B. Craine, D. C. Eteson, R. E. Grieves, W. Janischewskyj, G. W. Juette, and E. R. Taylor, "Radio noise design guide for high-voltage transmission lines," *IEEE Transactions on Power Apparatus and Systems,* vol. 90, no. 2, pp. 833–842, Mar. 1971.

[4] Electric Power Research Institute, *EPRI AC Transmission Line Reference Book—200 kV and Above*, 3rd ed. Palo Alto, California: Electric Power Research Institute, 2005, Chapter 9.

[5] Electric Power Research Institute, *EPRI AC Transmission Line Reference Book—345 kV and Above*, 2^{nd} ed. Palo Alto, California: Electric Power Research Institute, 1987, Chapter 5.

[6] R. J. Mather and B. M. Bailey, "Radio interference from high-voltage lines, Part I—statistical approach," *IEEE Transactions on Power Apparatus and Systems*, vol. 80, no. 3, pp. 890–894, Apr. 1961.

[7] R. J. Mather and B. M. Bailey. "Radio interference from high-voltage lines, Part II—distribution and correlation," *IEEE Transactions on Power Apparatus and Systems*, vol. 82, no. 68, pp. 775–782, Oct. 1963.

[8] V. L. Chartier, D. F. Shankle, and N. Kolcio, "The Apple Grove 750-kV Project: Statistical analysis of radio influence and corona-loss performance of conductors at 775-kV," *IEEE Transactions on Power Apparatus and Systems*, vol. 89, no. 5, pp. 867–881, May 1970.

[9] Y. Sawada, "Statistical study on radio noise of the 275-kV double conductors power transmission line," *Transactions of the Institute of Electrical Engineers of Japan A*, vol. 83, no. 902, pp.1897–1906, 1963.

[10] L. V. Timashova, "Statistical investigations of radio interference on 750 kV transmission lines," in *IEEE 1988 International Symposium on EMC,* 1988, pp. 424–429.

[11] H. H. Newell and F. W. Warburton, "Variations in radio and television interference from transmission lines," *IEEE Transactions on Power Apparatus and Systems*, vol. 75, no. 3, pp. 420–429, Jun. 1956.

[12] R. Bartenstein and E. Schafer, "Continuous measurements of the high-frequency interference level of HV transmission lines and their statistic evaluations," CIGRE, Paper 409, 1962.

[13] P. A. Abetti, J. J. LaForest, C. B. Lindh, and D. D. MacCarthy, "Results from the first year operation of project EHV," *IEEE Transactions on Power Apparatus and Systems*, vol. 81, no. 3, pp. 968–976, Apr. 1962.

[14] H. H. Newell, T. W. Liao, and F. W. Warburton, "Corona and RI caused by particles on or near EHV conductors: II – Foul weather," *IEEE Transactions on Power Apparatus and Systems*, vol. 87, no. 4, pp. 911–927, Apr. 1968.

[15] J. J. Laforest, "Seasonal variation of fair-weather radio noise," *IEEE Transactions on Power Apparatus and Systems*, vol. 87, no. 4, pp. 928–931, Apr. 1968.

[16] C. H. Gary and M. R. Moreau, "Predetermination of the radio noise level under rain of an extra-high-voltage line," *IEEE Transactions on Power Apparatus and Systems*, vol. 88, no. 5, pp. 653–660, May 1969.

[17] T. W. Schroeder, G. L. England, J. E. O'Neil, and W. E. Pakala, "345-kV wood-pole test line-radio influence and leakage-current investigations," *IEEE Transactions on Power Apparatus and Systems,* vol. 83, no. 3, pp. 228–236, Mar. 1964.

[18] O. Nigol, "Analysis of radio noise from high voltage lines, Parts I and II," *IEEE Transactions on Power Apparatus and Systems*, vol. 83, no. 5, pp. 524–541, May 1964.

[19] W. E. Pakala, V. L. Chartier, "Radio noise measurements on overhead power lines from 2.4 to 800 kV," *IEEE Transactions on Power Apparatus and Systems*, vol. 90, no. 3, pp. 1155–1165, May 1971.

[20] N. Kolcio, J. DiPlacido, R. J. Haas, D. K. Nichols, "Long term audible noise and radio noise performance of American electric power's operating 765 kV lines," *IEEE Transactions on Power Apparatus and Systems,* vol. 98, no. 6, pp. 1853–1859, Nov. 1979.

[21] *Radio Interference Characteristics of Overhead Power Lines and High-Voltage Equipment, Part 3: Code of Practice for Minimizing the Generation of Radio Noise*, CISPR 18-3, 1996.

[22] *IEEE Standard Definitions of Terms Relating to Corona and Field Effects of Overhead Power Lines,* IEEE Standard 539-2005, 2005.

[23] D. W. Marquardt, "An algorithm for least-squares estimation of nonlinear parameters," *Journal of the Society for Industrial and Applied Mathematics*, vol. 11, no. 2, pp. 431–441, Jun. 1963.

[24] J. Pujol, "The solution of nonlinear inverse problems and the Levenberg-Marquardt method," *Geophysics (SEG)*, vol. 72, no. 4, pp. W1–W16, DOI: 10.1190/1.2732552, Jul. 2007.

[25] F. J. Massey, "The Kolmogorov-Smirnov test for goodness of fit," *Journal of the American Statistical Association*, vol. 46, no. 253, pp. 68–78, Mar. 1951.

[26] K. T. Fang and J. L. Xu, *Statistical Distributions*. Beijing, China: Science Press, 1987, pp. 223–277.

Xie Huichun was born in 1980 in Shaoyan city, Hunan province, China. He received the B.S. degree in electrical engineering automation and M.S. degree in high voltage and insulation technology from Wuhan University in 2003 and 2006, respectively. Since 2011, he has been studying for his Ph.D. degree in electrical theory and new technology at North China Electric Power University. From 2006 to 2011, he worked in the State Grid Electric Power Research Institute as an engineer. In 2012, he joined the Chinese Electric Power Research Institute in his current position as a senior engineer. His research interests include electromagnetic environment and EMC and overvoltage in power system.

Xiang Cui (M'97–SM'98) was born in Baoding, Hebei Province, China, in 1960. He received the B.Sc. and M.Sc. degrees in electrical engineering from North China Electric Power University, Baoding, in 1982 and 1984, respectively, and the Ph.D. degree in accelerator physics from China Institute of Atomic Energy, Beijing, China, in 1988. He is currently a Professor and the Head of the Electromagnetic and Applied Superconductivity Laboratory, North China Electric Power University. His research interests include computational electromagnetic, electromagnetic environment and electromagnetic compatibility in power systems, insulation, and magnetic problems in high-voltage apparatus. Prof. Cui is an Associate Editor of IEEE Transactions on Electromagnetic Compatibility and a member of the editorial advisory board of the International Journal for Computation and Mathematics in Electrical and Electronic Engineering.

Baoquan Wan was born in Gansu Province, China, in 1971. He received the B.S. and Ph.D. degrees in electrical engineering from Wuhan University, Wuhan, China, in 2004 and 2007, respectively. Currently, he is a Professorial Senior Engineer and Master's Supervisor in China Electric Power Research Institute. His research interests are electromagnetic environment of high-voltage transmission lines and electromagnetic compatibility.

Zhang Jiangong was born in Hubei, China, in 1975. He received the B.S. degree in electrical engineering from Wuhan University of Hydraulic and Electrical Engineering, Wuhan, China, in 1999, and the M.S. degree in electrical engineering from Huazhong University of Science and Technology (HUST), Wuhan, China, in 2006. Currently, he is with the China Electric Power Research Institute (CEPRI), Wuhan, China. His research interests include power system electromagnetic compatibility and theelectromagnetic environment of power systems.